Special Feature: Vehicle Engineering

Research Report

Numerical Simulations of Aeroacoustic Fields around Automobiles

Yoshihiro Kato

Report received on Nov. 15, 2012

ABSTRACT Reduction of wind noise is necessary in the development of comfortable automobiles. In the present paper, a numerical approach and its applications to wind noise are introduced. The present method makes it possible to directly simulate aeroacoustic fields around automobiles. The approach employs the splitting method, which calculates flows and acoustic fields separately. The modeled acoustic equations are defined under the assumption that there is no acoustic feedback to the flows. The acoustic equations are calculated using the fourth-order weighted essentially non-oscillatory (WENO) scheme for the finite volume method, and a number of techniques are used to reduce the calculation time. The present paper first presents results for acoustic fields around a rear-view mirror on a flat plate. In addition, results around the mirrors on vehicle bodies are presented as a case study of mirror shapes. The results demonstrate that the present approach makes it possible to simulate wind noise directly, as well as showing how acoustic waves are generated and propagated around rear-view mirrors.

KEYWORDS Aeroacoustics, Aerodynamic Noise, Wind Noise, Computational Fluid Dynamics, Numerical Simulation, Wave, Noise

1. Introduction

In the development of automobiles, one important issue that affects passenger comfort is noise reduction. During high-speed driving, aerodynamic sounds are generated due to vortices in the air flow, which are often referred to as wind noise. The wind noise around the A-pillars and rear-view mirrors is especially uncomfortable because they are located near the passengers.

In automotive design, computational fluid dynamics (CFD) is widely used. Drag reduction and thermal analysis are major applications of CFD in automotive aerodynamics. Recently, CFD for aerodynamic sounds, or computational aeroacoustics (CAA), has been researched and developed. Although CAA is a rapidly progressing area, there are still many problems in its application to the acoustic fields around automobiles. One of the difficulties is that the fluctuations of the sound pressure are much smaller than those of the pressure induced by flow convection. Unless unsteady flows over 1 kHz (the sound frequency range) can be simulated precisely, the numerical errors disturb the solutions for acoustic fields. Another difficulty is that the characteristics of the sounds are different from those of the flows. The speed of sound is much greater than the flow speed in low-Mach-number flows. Because the time step in the calculation must be proportionately as small as the characteristic speed, it takes a very long time to simulate acoustic fields. For example, if the Mach number is 0.1, the calculation time is about 10 times as long as that for incompressible flows.

One of the approaches in CAA is using the splitting method such that each flow field and acoustic field is calculated separately. Incompressible flow fields are calculated, and then acoustic fields are calculated using the results of the flow fields. Since this splitting approach is not physically exact, there are several models that define aeroacoustic fields.

The popular approaches for CAA are based on Lighthill's acoustic analogy.[(1)] Many methods that use Lighthill's analogy employ analytically approximate solutions such as Curle's solution.[(2)] The assumptions in these methods are that the acoustic fields consist of only fields far from the source regions, and the source regions are smaller than the wavelength of the sounds (i.e., the sources are compact).

The wind noise produced around A-pillars and rear-view mirrors propagates and hits the body surface and

then reaches the passengers. Considering this process, the observation points are not in the far fields, and the sources are not compact. Thus, the assumptions based on Lighthill's analogy are not suitable for the acoustic fields around A-pillars and mirrors.

In the present paper, a method for simulating aeroacoustic fields around automobiles is introduced. Although this method is also a splitting method, the proper acoustic equations are used for the wind noise around automobiles. Similar splitting methods have been proposed by Hardin et al.[3] and Shen et al.[4]

The present approach focuses on how to simulate near fields and apply the simulations to practical objects like automobiles. For these purposes, an accurate acoustic model was defined, and stable numerical methods were employed to calculate the acoustic fields, including the regions near the sources. Furthermore, numerical techniques were developed to reduce the calculation time.

Using the present approach, it has become possible to simulate the acoustic fields around automobiles. The present paper introduces two examples of applications: one is a simulation around a rear-view mirror mounted on a flat plate,[5] and the other is around the A-pillars and the mirrors on the vehicle bodies.[6] The results can produce innovative visualizations that show how the wind noise is generated and propagated.

2. Nomenclature

c	: speed of sound
M	: Mach number
p	: pressure
Re	: Reynolds number
t	: time
u_i	: velocity
U_∞	: velocity of main flow
x_i, (x, y, z)	: coordinates
δ_{ij}	: Kronecker's delta
γ	: ratio of specific heat
ρ	: density
$\tilde{(\ )}$	: dimensional value
$\overline{(\ )}$	: time-average value
$(\ )_\infty$	: value of main flow
$(\ )_{rms}$	: root mean square

3. Numerical Methods

3. 1 Governing Equations

Various formulations exist for the splitting method, which calculates incompressible flows and acoustic fields separately. In the present study, the governing equations of the flow field are determined by the leading terms of the Mach number expansion discussed by Slimon et al.[7] The equations that are obtained from the leading terms for the mass and momentum equations are found to be the same as the incompressible flow equations. The acoustic density equation is obtained from the energy equation. This equation defines the density field as a function of the velocity and the pressure given by the incompressible flow equations. Therefore, the density in the flow field is a variable in the present study, although the flow field is assumed to be incompressible.

The compressible flow field (u_i, p, ρ) is assumed to be the sum of the incompressible flow field (u_{*i}, p_*, ρ_*) and the acoustic field (u_i', p', ρ') as follows:

$$u_i = u_{*i} + u_i', \quad p = p_* + p', \quad \rho = \rho_* + \rho' \quad \cdots\cdots\cdots (1)$$

The field (u_i', p', ρ') includes the pseudo-sound due to this splitting method. In the present study, however, this field is considered an "acoustic" field in order to observe the sound emission. Here, the dimensional values denoted by a tilde (e.g., $\tilde{u}_i$) are normalized to the following non-dimensional values:

$$u_i = \frac{\tilde{u}_i}{\tilde{U}_\infty}, \quad p = \frac{\tilde{p} - \tilde{p}_\infty}{\tilde{\rho}_\infty \tilde{U}_\infty^{\,2}}, \quad \rho = \frac{\tilde{\rho} - \tilde{\rho}_\infty}{\tilde{\rho}_\infty} \quad \cdots\cdots\cdots (2)$$

The variables (u_{*i}, p_*, ρ_*) satisfy the incompressible flow equations. Then, the density equation and the momentum acoustic equations with the variables (u_i', p', ρ') are written as follows:

$$\frac{\partial \rho'}{\partial t} + \frac{\partial f_j}{\partial x_j} = -\frac{D_* \rho_*}{Dt}, \qquad \cdots\cdots\cdots (3)$$
$$f_j = (1 + \rho_* + \rho')u_j' + \rho' u_{*_j},$$

$$\frac{\partial f_i}{\partial t} + \frac{\partial h_{ij}}{\partial x_j} = -\frac{D_* \rho_* u_{*_i}}{Dt}, \qquad \cdots\cdots\cdots (4)$$
$$h_{ij} = f_i(u_{*_j} + u_j') + (1 + \rho_*)u_{*i}u_j' + p'\delta_{ij},$$

where the viscous terms in the momentum equation are

neglected, and D_*/Dt denotes the substantial derivative. The acoustic field is assumed to be isentropic and employs the following relationship between p' and ρ':

$$p' = c_*^2 \rho'. \quad \cdots\cdots\cdots\cdots\cdots\cdots\cdots\cdots (5)$$

The speed of sound c_* is a non-dimensional variable normalized by the reference velocity $\tilde{U}_\infty$, which is written as follows based on Eq. (2):

$$c_*^2 = \gamma \frac{1}{1+\rho_*}\left(p_* + \frac{1}{\gamma M_\infty^2}\right). \quad \cdots\cdots\cdots\cdots\cdots (6)$$

As mentioned above, the density ρ_* in the flow field is obtained from the energy equation through the Mach number expansion. However, the present study uses its approximation,[8] which is

$$\rho_* = M_\infty^2 p_*. \quad \cdots\cdots\cdots\cdots\cdots\cdots\cdots\cdots (7)$$

The results of the incompressible flow calculations are substituted into Eqs. (3) and (4) for acoustic fields, which are then integrated with the time marching scheme.

3. 2 Applicability of Splitting Methods

The incompressible flow field (u_{*i}, p_*) can be calculated by conventional numerical methods. Then, ρ_* is given by Eq. (7), and the acoustic field can be calculated by the present acoustic model. Consequently, these calculations give the solutions of compressible flows because the present model is defined as Eq. (1). This means that the present method is an easier procedure for calculating compressible flows with low Mach numbers than the direct simulations of compressible flows.

Because the flow and acoustic fields are calculated separately, splitting methods are generally based on an important assumption that the acoustic fields do not change the flow fields. Such a change is referred to as feedback. In fact, many kinds of aerodynamic noise are caused by feedback. For example, the edge tone and wind throb around automobile sunroofs are feedback noises. These flows with feedback noise are not governed by the incompressible flow equations. Therefore, splitting methods can be used to simulate flows that can be calculated with incompressible flow equations.

3. 3 Numerical Schemes

Since the governing equations for both flow and acoustic fields can be written in generalized coordinates, they can be applied to the fields around practical objects like automobiles. Since Eqs. (3) and (4) require time derivatives, the accuracy of the fluctuating variables in the calculation of the flows significantly affects the accuracy of the acoustic field calculation. In the present study, the large eddy simulation (LES) with the mixed-time-scale SGS model by Inagaki et al.[9] is used to calculate the flow fields. The discretization method is the finite volume method (FVM) on collocated grids.[10] The spatial derivative is approximated by the second-order central difference; the time integration is performed with the Crank–Nicolson implicit scheme. The pressure fields are calculated in the same manner as the simplified marker and cell (SMAC) method. The numerical scheme used for the flow field in this paper has been validated in numerous test calculations.[11]

The acoustic fields are calculated using the FVM with the weighted essentially non-oscillatory (WENO) scheme.[12] The solution vectors on both sides of each cell face are calculated using the fourth-order WENO scheme, and the numerical fluxes on the cell faces are calculated using the Harten–Lax–van Leer–Einfeldt (HLLE) method,[13] which is an approximate Riemann solver, in the same manner as in Ref. (14). Time integration is performed using the two-step Runge–Kutta scheme.

The present numerical methods have been applied to the acoustic fields around a circular cylinder[8] and a three-dimensional rectangular cylinder[14] by the author. The result for the circular cylinder showed that the present calculation can correctly predict the pseudo-sound components included in p'. The result of the rectangular cylinder demonstrated that the increments in the sound pressure levels with the height of the rectangular cylinders are in good agreement with the measurements.

4. Aeroacoustic Fields around a Rear-view Mirror on a Flat Plate

4. 1 Geometry

The shape of the rear-view mirror in the present simulation is shown in **Fig. 1**. This shape is simplified, while actual rear-view mirrors have a dished shape and

a clearance to allow for folding. The rear-view mirror is mounted on a large flat plate in a uniform flow. Each of the computational regions used for flow and acoustic calculations are shown in **Fig. 2**. The computational regions are different because each region needs a suitable width to calculate each field efficiently.

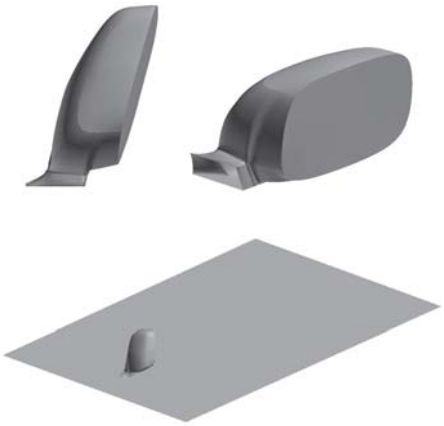

Fig. 1 Model.

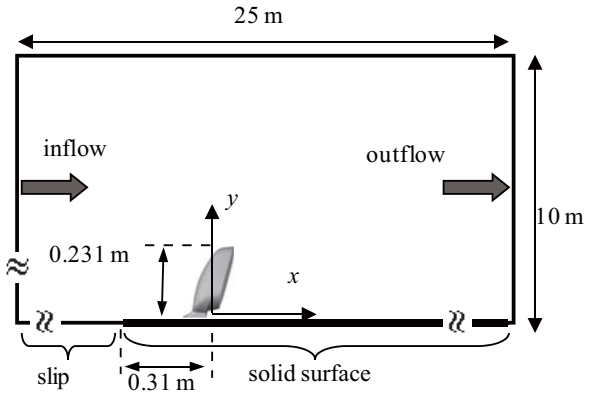

(a) Flow field

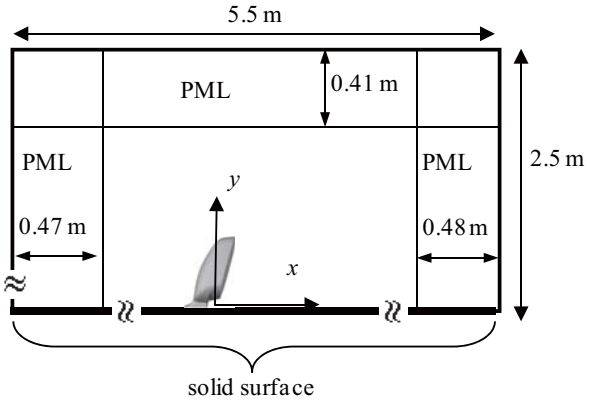

(b) Acoustic field

Fig. 2 Computational regions (*x*-*y* plane).

4. 2 Computation of Flow

A sketch of the computational domain with the boundary conditions used in the flow calculations is shown in Fig. 2(a). The boundary condition of the solid surfaces is the three-layer wall condition,[15] which is a modification of the two-layer wall condition of Werner et al.[16] The inflow condition is a uniform flow. The outflow condition for the velocity has a spatial gradient equal to zero. The pressure at the outflow boundary is set to $p_* = 0$, and Neumann conditions are implemented for the other boundaries.

A single-block structured grid is used over the entire region. The grid spacing in the normal direction from the wall to the first point is 0.4 mm. There are 309 × 143 × 159 grid points in the *x*, *y*, and *z* directions, respectively. The main flow velocity is 38.9 m/s, and the Reynolds number based on a reference length of 0.1 m and the main flow velocity is 253,000. Under these conditions, the Mach number is equal to 0.113.

The computed velocity vectors are shown in **Fig. 3**. This figure shows an instantaneous flow field. Strong small vortices are generated from the shear flows around the tip and the neck. These vortices cause the wind noise.

4. 3 Computation of Acoustics

In general, in computing flow fields, small grid spacing must be used in regions close to solid surfaces to increase the spatial resolution. For acoustic fields, such high resolution near solid surfaces is not required, because the viscous terms in the acoustic equations are neglected.

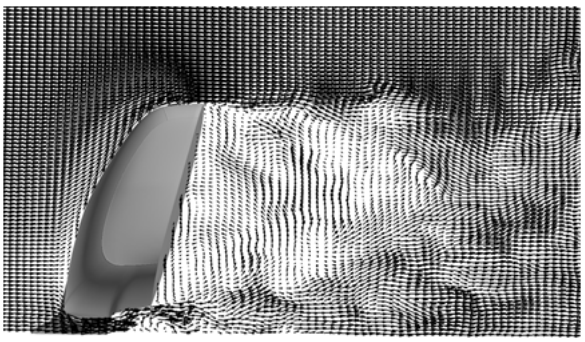

Fig. 3 Velocity vectors (instantaneous field).

Consequently, different grid systems are used for the flow and acoustic calculations, in the same manner as in Ref. (14). Here, the spacing of the first point from the solid surface is set to 1 mm for the acoustic grid. The computational region is shown in Fig. 2(b) along with the boundary condition settings. There are 283 × 150 × 160 grid points in the x, y, and z directions, respectively. Both flow and acoustic calculations are performed in generalized curvilinear coordinates. The computed flow field parameters are remapped from the flow grid onto the acoustic grid using trilinear interpolation.

The present acoustic calculations use the perfectly matched layer (PML) approach,[17] which guarantees no reflections at the outer boundaries. The dumping function in the PML approach is used as described in Ref. (8); it is proportional to the square of the distance from the inner edges of the PML. The boundary conditions at the body surface and the ground plate are full reflective.

If the same time step is used for acoustics and flow in the aforementioned grid systems, and the Courant number is set to 0.25 for acoustics, the Courant number for flow is 0.0625. Despite the use of different grid spacings, the time step is still small in the flow calculation. Here, the reference velocity for flow is the uniform flow velocity, and that for acoustics is the sum of the uniform flow velocity and the speed of sound.

For this problem, for each time step calculated for the flow, four time steps are calculated for the acoustics. To match the computed data, a cubic function is used to interpolate the variables of Eqs. (3) and (4) at four time levels while maintaining continuous gradients. The time step for flow is 2.56×10^{-6} seconds, and that for acoustics is 0.64×10^{-6} seconds.

The present study addresses the sound simulation in the region from 1 kHz to 2 kHz. The time step is much smaller than 5.0×10^{-4} seconds, which corresponds to 2 kHz, and therefore, the time interpolation does not reduce the accuracy.

4 .4 Characteristics of Sound Emission

Some numerical results related to the acoustic field are shown in **Fig. 4**. Figure 4(a) displays the distribution of pressure in the x-y plane near the central cross section of the rear-view mirror, and Fig. 4(b) represents the distribution of pressure on the ground plane. The distributions are shown for the entire computational region. It can be seen that the computed results are reliable because behaviors not found in the real world (e.g., reflections from the outer boundary) are not present in the figure.

The instantaneous distribution of sound pressure is shown in **Fig. 5** in order to visualize how the sounds are emitted to the far field. The sound pressure given in the figure is filtered by a frequency band from 1 kHz to 2 kHz to cut off the low-frequency fluctuations generated by the flow convection. Regions with low pressure (and consequently low density) are indicated by light coloration, while the regions of high pressure

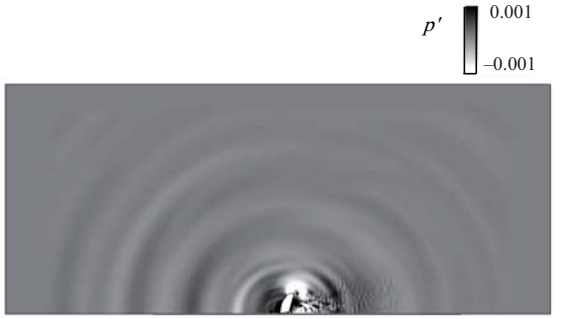

(a) x-y plane

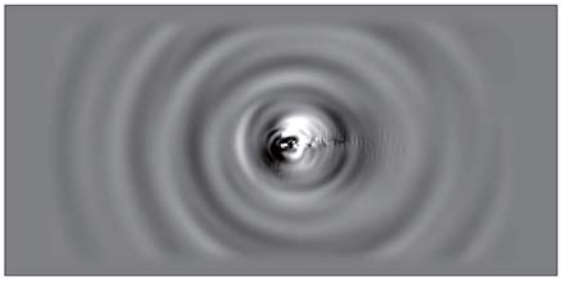

(b) x-z plane (ground plane)

Fig. 4 Acoustic field.

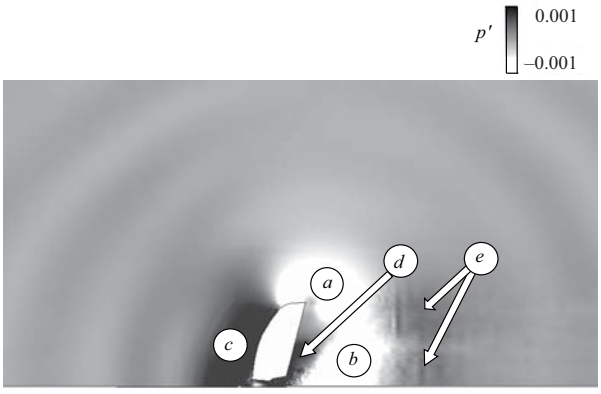

Fig. 5 Acoustic field with a filter between 1 kHz and 2 kHz.

are indicated by dark coloration. From the figure, we see that the low-density regions are in the domains labeled *a* and *b*; these indicate the generation of vortices from the shear layers seen in Fig. 3. The vortex generation causes pulsation of the high-density domains indicated by *c*, *d*, and *e*; as a result of this, sound is emitted. These high-density domains are seen around stagnation of the flow; the location of the upper part of the *e*–domain corresponds to the confluence of the flow from the neck and the tip.

Once the fields p' and u_i' are computed, it is possible to calculate acoustic intensity vectors using the following equation:[14]

$$I_i = \overline{(p' - \overline{p'})(u_i' - \overline{u_i'})}. \quad \cdots\cdots\cdots\cdots\cdots\cdots (8)$$

The direction of sound propagation can be investigated by drawing streamlines in the field of acoustic intensity vectors (hereinafter, these lines are referred to as "acoustic streamlines").

Figure 6 shows the acoustic streamlines. In this study, the governing equations of acoustics are defined as the difference between the compressible and incompressible equations. By this definition, the sound pressure in the far field is radiated like a wave. In contrast, that of the near field is influenced by convection and is produced like the flow field pressure distribution, as shown in Fig. 5.

Figure 6(a) shows the acoustic field over the entire range of frequencies. In Fig. 5, the frequency filter is effective at visualizing the acoustic field. The field for acoustic streamlines is also filtered for the range of frequencies from 1 kHz to 2 kHz, and the result is shown in Fig. 6(b). The acoustic streamlines in the wake in Fig. 6(b) propagate diagonally in the upper-right direction between the mirror and ground. The paths of the lines are more radial than those in Fig. 6(a). The wave characteristics can appear in the wake by means of the high-pass filter.

The sound propagating diagonally in the downstream direction is emitted from the neck of the mirror through the shear flow downstream of the tip. The results shown in Fig. 5 indicate that the wave propagating in the upward and right directions is caused by the flow fluctuation at locations *d* and *e*.

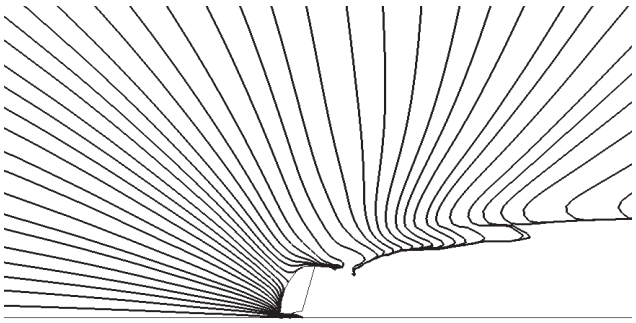

(a) Overall

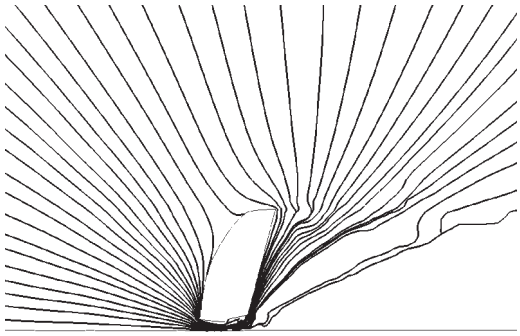

(b) With a filter between 1 kHz and 2 kHz

Fig. 6 Acoustic streamlines.

5. Aeroacoustic Fields around Rear-view Mirrors on Vehicle Bodies

5. 1 Shapes and Computational Conditions

The automobile model is shown in **Fig. 7**. The model has a simplified shape, including a flat floor, and the wheels are modeled as filleted circular cylinders. The total model length is 4.4 m. The model includes the bump of the A-pillar. The rear-view mirror is also simplified, as shown in Fig. 7. For the validation of the present method, a case study using different mirror shapes is performed. The mirror shape in Fig. 7 is the

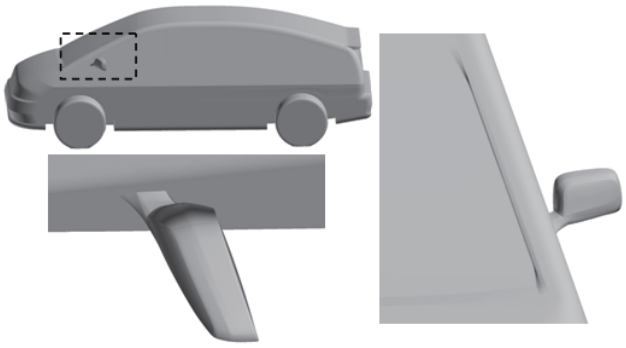

Fig. 7 Model.

baseline and is referred to as Case 1. The baseline mirror is shown in **Fig. 8**(a). The other two models are shown in Figs. 8(b) and (c) and are referred to as Cases 2 and 3, respectively. Their shapes are intended to produce large wind noise. The cross section of the stay in Case 2 is sharper than that in Case 1. The noise in Case 2 is assumed to be greater than that in Case 1 because the flow separation generates strong vortices at the stay. On the other hand, the shape of the tip is different in Case 3. Since flow separation occurs at the front face of the tip, the noise in Case 3 is assumed to be greater than that in Case 1.

The main flow velocity is 38.9 m/s, and the Reynolds number is 2.53 million. The reference length is 1 m, and the reference velocity is the main flow velocity. The Mach number is 0.113 in this main flow. The wheels are rotated, and the ground moves at the main flow speed relative to the automobile body. The calculations for the half model are performed using the symmetric boundary condition.

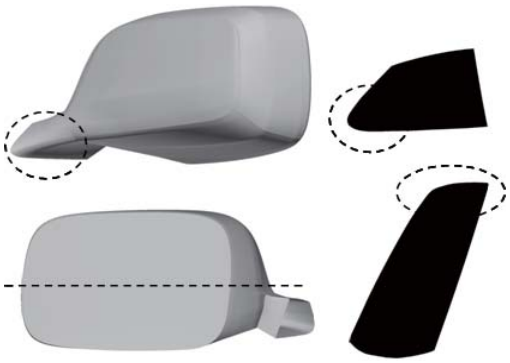

(a) Case 1 (baseline)

(b) Case 2 (sharp stay)

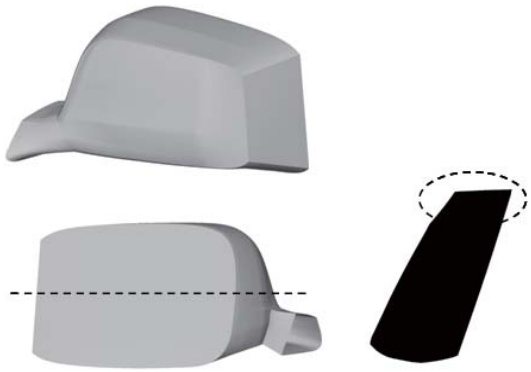

(c) Case 3 (sharp tip)

Fig. 8 Mirror shapes used in the case study.

5. 2 Computation of Flow

Sketches of the computational grids for the flow simulations are shown in **Fig. 9**. The grid system is an overset grid system with three structured grids. The first grid is around the A-pillar and the rear-view mirror, the second grid is around the entire body, and the third grid covers the entire region. The first grid has a fine resolution; the grid spacing normal to the wall for the first point is approximately 0.4 mm. The total number of grid points is 27.5 million.

5. 3 Computation of Aeroacoustics

Reducing the calculation time for aeroacoustic fields is important primarily because the time step size for acoustic calculations (Δt_{ac}) is much smaller than that for flow calculations (Δt_{flow}). This is because the speed of sound is much greater than the speed of the flow. In

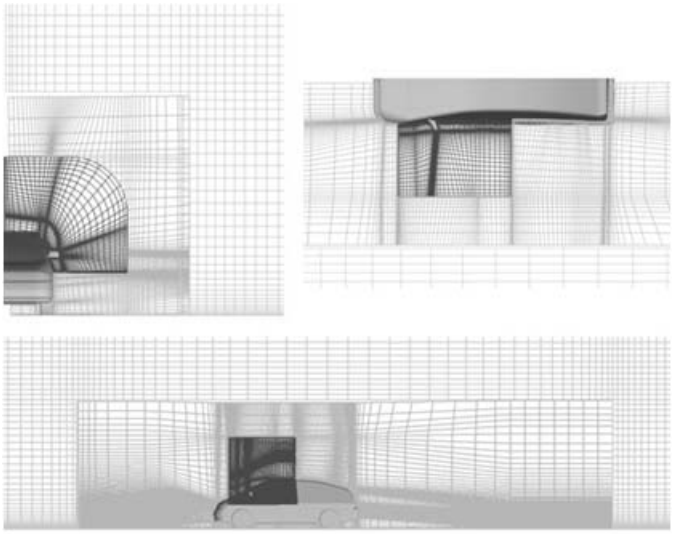

Fig. 9 Computational grids for flow simulations. (In the grid around the A-pillar and the mirror, every fifth grid line is shown, and in the grid around the body, every third grid line is shown.)

order to address this problem, the following three techniques, which take advantage of flow/acoustic splitting, are used.

The first technique involves the use of a different mesh spacing in each acoustic and flow calculation. In general, small mesh spacing is required near walls in flow calculations because the boundary layers require high resolution. In the Courant–Friedrichs–Lewy (CFL) condition, Δt_{ac} is approximately $\Delta t_{flow} M$ and is very small in low-Mach-number flows if the same grid is used as for the flows. Therefore, the cost increases approximately 10 times for flows with $M = 0.1$. As for acoustic fields, such high resolution near solid surfaces is not required, because the viscosity appears not to be important. In the present acoustic model, the viscous terms are neglected. If the mesh spacing for acoustics near the wall can be set to be greater than that for the flows, the calculation time can be reduced. In the present computations, the mesh spacing of the first point from the solid surface is set to approximately 2 mm for acoustics. Since the mesh spacing is five times greater than that of the flow calculation, a large time step size can be set. In order to use different meshes in the acoustic and flow calculations, the values of the computed flows must be interpolated to the acoustic grids. In the present computations, the trilinear interpolation method is used.

The second technique involves the use of different time step sizes where the same time step size is not required for acoustics and flows. The calculations for the rear-view mirrors run only one time step for flows during the time required for four steps for acoustics. Thus, the calculation time for flows can be reduced. The time step size for flows in the present calculations is 1.928 microseconds, whereas that for acoustics is 0.482 microseconds. The Courant number is 0.1875 for flows and 0.0923 for acoustics. Here, the reference velocity for flows is the main flow velocity, and that for acoustics is the sum of the main flow velocity and the speed of sound. Although these time step sizes are small because of the low quality of the meshes, using different time step sizes is effective at reducing the calculation time.

The third technique limits the computational regions. The present aeroacoustic fields defined by Eqs. (3) and (4) are mostly wave fields far from sound sources, although the near fields exhibit nonlinearity. At a certain distance from the rear-view mirrors, the directions of the acoustic pressure radiation are mostly toward the outside. The boundaries can be located in such regions in which no vortices are generated around the mirrors. This means that the boundaries for acoustics can be different from those for flows, and the acoustic computational regions can be smaller than those for flows. **Figure 10** shows the computational grid for acoustics. The acoustic calculations are conducted only inside this grid. The number of grid points is 10.2 million.

At boundaries other than the solid surface, the non-reflecting condition is imposed using PML. Since there are vortical flows from upstream of or around the front wheels, the limited regions are not actually suitable for the non-reflecting boundary condition. However, limitation of the regions has two significant advantages: 1) the reduction in calculation time associated with the reduction in the number of grid points, and 2) the prevention of spurious noise. Sound waves essentially propagate over far fields. If the entire region around an automobile is calculated, sounds emitted from any region may reach the observation points. Therefore, the spurious noise radiated from far areas affects the results around the observed area if the calculations are not precise in the entire region. For example, if there is a large numerical error around the wheel as a result of a coarse grid, spurious noise may be generated and may reach the rear-view mirrors. For these reasons, limitation of the regions is required in order to calculate the acoustic fields for complicated objects, such as the acoustic fields around automobiles.

The present calculations are performed on the Earth

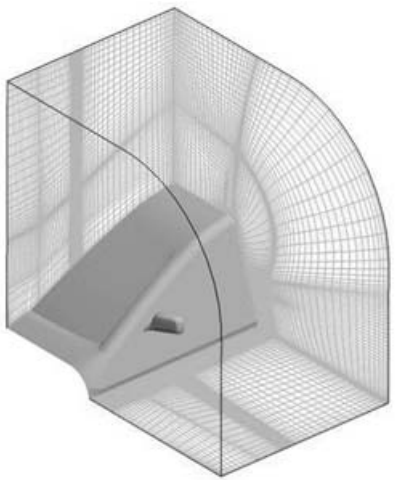

Fig. 10 Computational grid for acoustics simulation. (Every third line is shown.)

Simulator, which is a large system of vector-type processors. In a typical case, the simulation time is 0.0289 seconds. If eight processors of one node are used, the total elapsed calculation time is approximately 42 hours for one case. The flow calculation takes 36 hours, and the acoustic calculation takes 6 hours. The flow calculation takes longer than usual because the residual in the iterative calculations must be reduced more than in the case for typical flow simulations to reduce the error in the law of mass conservation. The calculation time may be reduced if the convergence performance of the solver is improved.

5. 4 Flow Fields

A case study is conducted in order to investigate the acoustic field variation, which depends on the shape of the mirror. The calculated velocity vectors are shown in **Figs. 11** and **12**, and the root mean square (RMS) pressure fluctuations are shown in **Fig. 13**. Here, the RMS pressure fluctuation is given as follows:

$$p_{RMS} = \left(\overline{(p - \overline{p})^2} \right)^{1/2}, \quad \cdots\cdots\cdots\cdots\cdots\cdots (9)$$

where $\overline{p}$ is the time average of p. The RMS pressure fluctuations for p_* and p' are denoted as p_{*RMS} and p'_{RMS}, respectively.

In Case 2, the flow separates beneath the mirror and vortices are generated, as shown in Fig. 11(b). Therefore, the pressure fluctuation increases beneath the mirror, as shown in Fig. 13(b). Similarly, the separation at the tip shown in Fig. 12(b) increases the pressure fluctuation, as shown in Fig. 13(c). Figures 11, 12, and 13 indicate that the mirrors in Cases 2 and 3 must generate greater noise than that in Case 1. The following acoustics computations will indicate whether reasonable results can be obtained.

5. 5 Aeroacoustic Fields

The calculated acoustic pressure fields (p') are shown in **Figs. 14**, **15**, and **16**. In the visualizations shown in

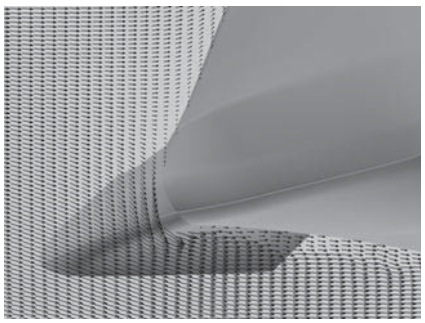

(a) Case 1

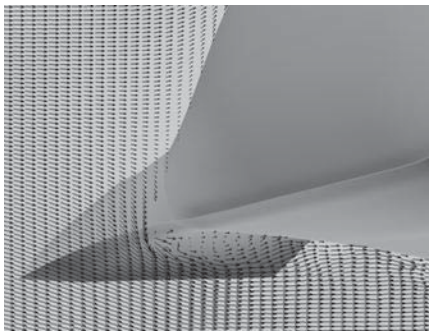

(b) Case 2

Fig. 11 Velocity vectors on the vertical plane (instantaneous field).

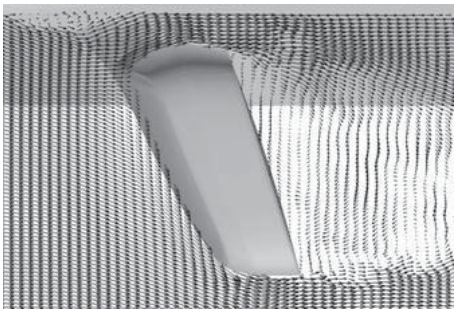

(a) Case 1

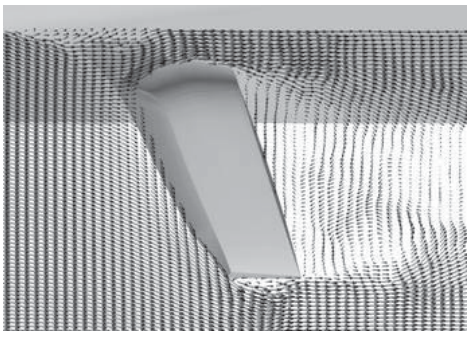

(b) Case 3

Fig. 12 Velocity vectors on the horizontal plane (instantaneous field).

Figs. 14 and 15, some of the fluctuation patterns move slowly (at the speed of convection), and some propagate as fast as sound waves. The origins and propagations of the wind noise can be observed directly from the visualizations.

In Case 2, strong waves are emitted from the neck of the mirror, as expected from the flow fields. These waves are the strongest among all of the cases. Downward directivity is indicated by the strong fluctuation around the underside of the stay in Fig. 13(b).

In Case 3, the waves are stronger than those in Case 1. However, these waves are weaker than those in Case 2 because the high-fluctuation area is smaller than that for Case 2, as shown in Fig. 13. The origin of the waves can be seen around the tip. Thus, the propagation of Case 3 is different from that of Case 2.

The sound emission can be observed around the A-pillars. In Fig. 15, the sources around the A-pillars appear near the front of the mirrors, and other sources appear above the mirrors in Cases 2 and 3. The

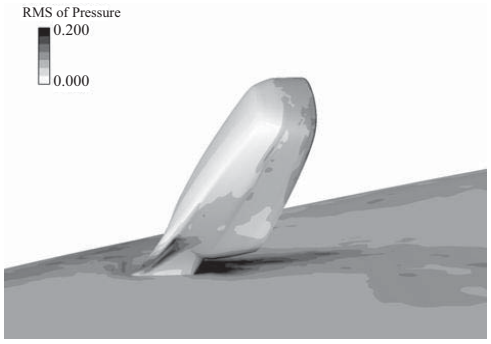

(a) Case 1

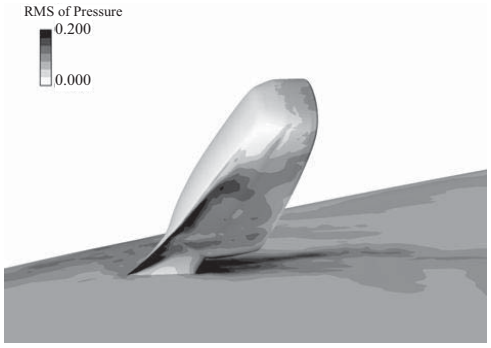

(b) Case 2

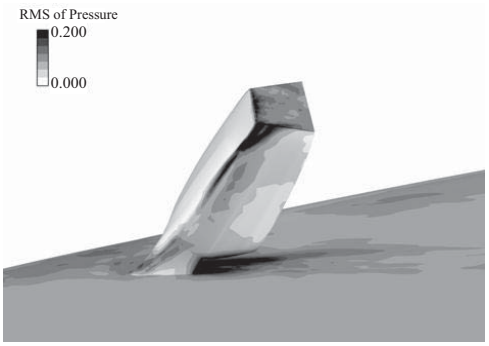

(c) Case 3

Fig. 13 Distributions of p_{*RMS}.

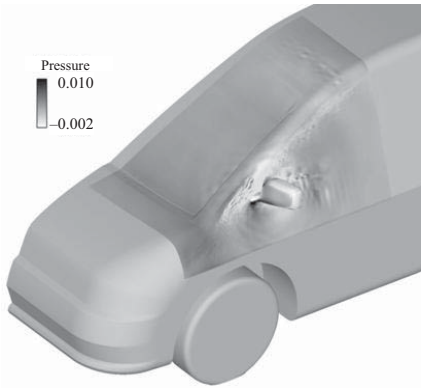

(a) Case 1

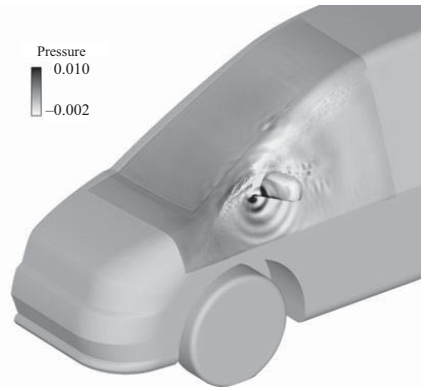

(b) Case 2

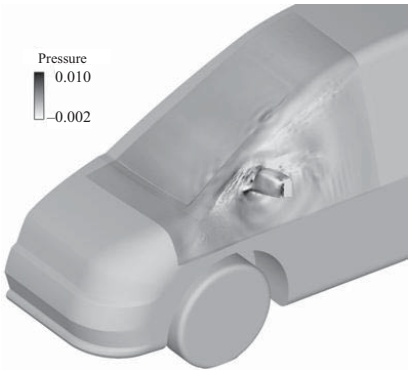

(c) Case 3

Fig. 14 Acoustic pressure fields (overall view).

locations and strengths of the origins are not the same in each case because the strong vortices around the neck or tip appear to change the flows around the A-pillars.

Upon closer inspection, Fig. 14 reveals that the incident waves move inward from the outer boundaries, although they are not clear in the instantaneous figures. Since these waves are caused by the limited computational regions, the waves arise due to numerical errors and are undesirable. In particular, at the downward boundaries, the flow fluctuations around the front wheels generate the waves. Although the waves actually exist, the frequency is low, and the level is not significant in the present case study. Generally, it is necessary to select the regions carefully for acoustic simulations if the regions are limited to a small area.

Consequently, these calculation results show that the present method can simulate wind noise with sufficient accuracy to find the variation caused by the vortices

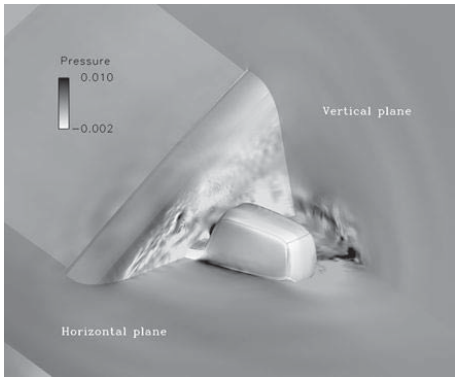

(a) Case 1

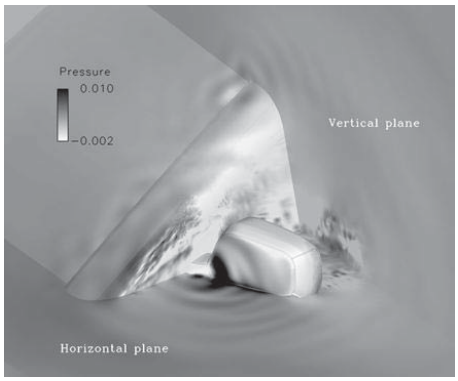

(b) Case 2

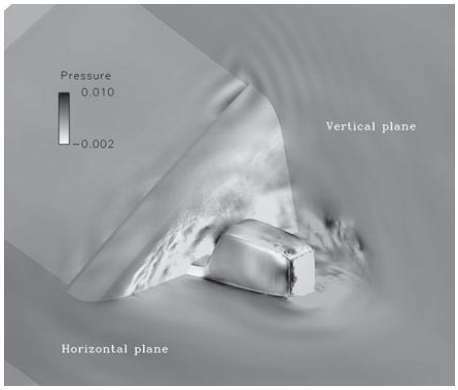

(c) Case 3

Fig. 15 Acoustic pressure fields (near view).

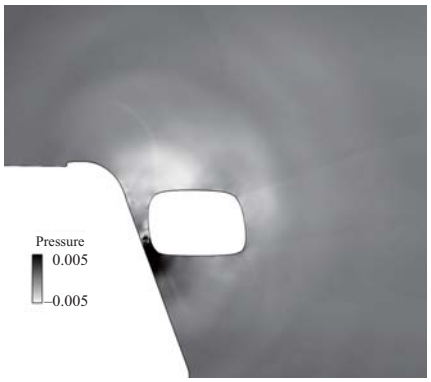

(a) Case 1

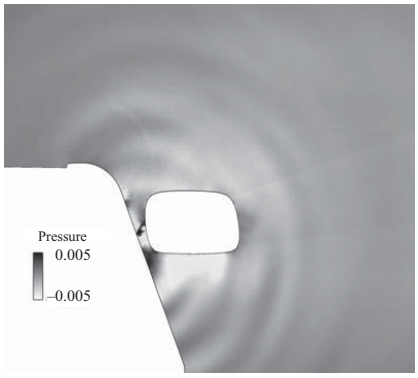

(b) Case 2

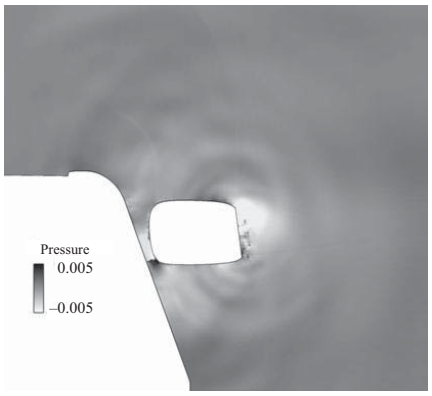

(c) Case 3

Fig. 16 Acoustic pressure fields (front view).

due to flow separations. The results appear to be physically reasonable. Direct validation by measurement has not yet been conducted and is a subject of future research.

6. Conclusions

The present paper introduced a method to simulate the aeroacoustic fields directly around automobile rear-view mirrors. The method uses the splitting technique, which calculates incompressible flows and acoustic fields separately. The major assumption is that acoustic disturbances do not change the vortical flow fields. Therefore, it cannot be applied to the feedback noise, such as the edge tone and wind throb around the sunroof. The criterion is that the convective motion of flow can be governed by incompressible flow equations. In many low-Mach-number flows with aerodynamic sounds, the flows are governed by the incompressible flow equations. Therefore, this splitting method can be used for many applications, not only for automobiles but also for other objects.

The numerical methods for the present acoustic calculations employ the fourth-order WENO scheme for the FVM and the PML for the non-reflecting condition at the outer boundaries. In addition, the present paper introduced some techniques to reduce the calculation time.

The numerical results demonstrated clearly how the wind noise is generated and propagated around automobile rear-view mirrors. The simulation of the mirror on a flat plate shows the acoustic field that is generated due to the wake of the mirror with a frequency around 1 kHz to 2 kHz. Moreover, the simulations around the A-pillars and the mirrors mounted on the bodies demonstrated that acoustic fields are generated due to the separated flows around the mirror stay and the tip with a frequency around 4 kHz.

The proposed method was successful in visualizing the acoustic fields around A-pillars and rear-view mirrors. If the acoustic fields are calculated directly, the results can be used for the calculations of the transmitted sounds, which reach the passengers from the outside. Although including structural issues is very difficult, a complete wind noise simulation will be possible with further progress in CAA.

Acknowledgments

The computations discussed in the present study were performed using the Earth Simulator of the Japan Agency for Marine-Earth Science and Technology.

References

(1) Lighthill, M. J., “On Sound Generated Aerodynamically I. General Theory”, *Proceedings of the Royal Society of London A*, Vol. 211 (1952), pp. 564-587.
(2) Curle, N., “The Influence of Solid Boundaries upon Aerodynamic Sound”, *Proceedings of the Royal Society of London A*, Vol. 231 (1955), pp. 505-514.
(3) Hardin, J. C. and Pope, D. S., “An Acoustic/viscous Splitting Technique for Computational Aeroacoustics”, *Theoretical and Computational Fluid Dynamics*, Vol. 6 (1994), pp. 323-340.
(4) Shen, W. Z. and Sorensen, J. N., “Aeroacoustic Modelling of Low-speed Flows”, *Theoretical and Computational Fluid Dynamics*, Vol. 13 (1999), pp. 271-289.
(5) Kato, Y., Men'shov, I. and Nakamura, Y., “Aeroacoustics Simulations around Automobile Rear-view Mirrors”, *Journal of Fluid Science and Technology*, Vol. 3, No. 7 (2008), pp. 892-905.
(6) Kato, Y., “Numerical Simulations of Aeroacoustic Fields around Automobile Rear-view Mirrors”, *SAE International Journal of Passenger Cars - Mechanical Systems*, Vol. 5, No. 1 (2012), pp. 567-579.
(7) Slimon, S. A., et al., “Development of Computational Aeroacoustics Equations for Subsonic Flows Using a Mach Number Expansion Approach”, *Journal of Computational Physics*, Vol. 159 (2000), pp. 377-406.
(8) Kato, Y., Men'shov, I. and Nakamura, Y., “Aeroacoustic Simulation around a Circular Cylinder by the Equations Split for Incompressible Flow Field and Acoustic Field”, *Transactions of the Japan Society of Mechanical Engineers, Series B* (in Japanese), Vol. 71, No. 711 (2005), pp. 2694-2701.
(9) Inagaki, M., et al., “A Mixed-time-scale SGS Model with Fixed Model-parameters for Practical LES”, *Journal of Fluids Engineering*, Vol. 127 (2005), pp. 1-13.
(10) Inagaki, M. and Abe, K., “An Improvement of Prediction Accuracy of Large Eddy Simulation on Colocated Grids”, *Transactions of the Japan Society of Mechanical Engineers, Series B* (in Japanese), Vol. 64, No. 623 (1998), pp. 1981-1988.
(11) Inagaki, M., et al., “Predictions of Wall-pressure Fluctuation in Separated Complex Flows with Improved LES and Quasi-DNS”, *Proceedings of the 3rd International Symposium on Turbulence and Shear Flow Phenomena*, Vol. III (2003), pp. 941-946.
(12) Liu, X. -D., et al., “Weighted Essentially Non-

oscillatory Schemes", *Journal of Computational Physics*, Vol. 115 (1994), pp. 200-212.
(13) Davis, S. F., "Simplified Second-order Godunov-type Methods", *SIAM Journal on Scientific and Statistical Computing*, Vol. 9, No. 3 (1988), pp. 445-473.
(14) Kato, Y., Men'shov, I. and Nakamura, Y., "Aeroacoustic Simulation around a Rectangular Cylinder on the Ground Surface", *Transactions of the Japan Society of Mechanical Engineers, Series B* (in Japanese), Vol. 72, No. 716 (2006), pp. 956-963.
(15) Inagaki, M., et al., "Numerical Prediction of Fluid-resonant Oscillation at Low Mach Number", *AIAA Journal*, Vol. 40, No. 9 (2002), pp. 1823-1829.
(16) Werner, H. and Wengle, H., "Large Eddy Simulation of Turbulent Flow over and around a Cube in a Plate Channel", *Proceedings of the 8th Symposium on Turbulent Shear Flows*, Vol. 2 (1991), pp.(19-4-1)-(19-4-6).
(17) Hu, F. Q., "On Perfectly Matched Layer as an Absorbing Boundary Condition", *Proceedings of the 2nd AIAA/CEAS Aeroacoustics Conference*, *AIAA Paper* No. 96-1664 (1996).

Figs. 1, 2, 4-6, Sections 2, 3.1, 3.3 and 4
Reprinted from Journal of Fluid Science and Technology, Vol. 3, No. 7 (2008), pp. 892-905, Kato, Y., Men'shov, I. and Nakamura, Y., Aeroacoustics Simulations around Automobile Rear-view Mirrors, © 2008 The Japan Society of Mechanical Engineers.

Section 5
Reprinted from SAE paper 2012-01-0586 (SAE International Journal of Passenger Cars - Mechanical Systems, Vol. 5, No. 1) (2012), Kato, Y., Numerical Simulations of Aeroacoustic Fields around Automobile Rear-view Mirrors, © 2012 SAE International, with permission from SAE International.

Yoshihiro Kato
Research Fields:
- Aerodynamics
- Aeroacoustics
- Computational Fluid Dynamics

Academic Degree: Dr.Eng.
Academic Societies:
- The Japan Society of Mechanical Engineers
- Society of Automotive Engineers of Japan

